Structural Engineering and Mechanics, *Vol. 59, No. 4 (2016) 683-701*
DOI: http://dx.doi.org/10.12989/sem.2016.59.4.683

A framework for carrying out train safety evaluation and vibration analysis of a trussed-arch bridge subjected to vessel collision

Chaoyi Xia[1,2], Nan Zhang[1,2], He Xia[*1,2], Qin Ma[3] and Xuan Wu[1]

[1]*School of Civil Engineering, Beijing Jiaotong University, Beijing 100044, China*
[2]*Beijing Key Laboratory of Track Engineering, Beijing 100044, China*
[3]*CCCC Highway Consultants Co., Ltd., Beijing 100088, China*

(Received November 17, 2015, Revised May 4, 2016, Accepted June 15, 2016)

Abstract. Safety is the prime concern for a high-speed railway bridge, especially when it is subjected to a collision. In this paper, an analysis framework for the dynamic responses of train-bridge systems under collision load is established. A multi-body dynamics model is employed to represent the moving vehicle, the modal decomposition method is adopted to describe the bridge structure, and the time history of a collision load is used as the external load on the train-bridge system. A (180+216+180) m continuous steel trussed-arch bridge is considered as an illustrative case study. With the vessel collision acting on the pier, the displacements and accelerations at the pier-top and the mid-span of the bridge are calculated when a CRH2 high-speed train running through the bridge, and the influence of bridge vibration on the running safety indices of the train, including derailment factors, offload factors and lateral wheel/rail forces, are analyzed. The results demonstrate that under the vessel collision load, the dynamic responses of the bridge are greatly enlarged, threatening the running safety of high-speed train on the bridge, which is affected by both the collision intensity and the train speed.

Keywords: trussed-arch bridge; vessel collision load; high-speed train; dynamic response; running safety evaluation

1. Introduction

According to the statistics by Wardhana and Hadipriono (2003) on 503 bridge collapse accidents in the United States during 1989 to 2000, there were 59 accidents caused by collisions, which were 11.7% of the total, only preceded by floods (Fig. 1). A review by Harik *et al*. (1990) on 79 bridge failures in the United States over a 38-years period (1951-1987) indicated that 36 events (45.6%) of them were due to collisions, in which more than half (19 events) were caused by vessel collisions.

A similar investigation by Dong *et al*. (2009) on 502 bridge collapse accidents in 66 countries reported 91 accidents caused by various collisions (vessels, trains, trucks and some floating objects), constituting 18% of the total bridge collapses. While in the 91 collision accidents, 56

*Corresponding author, Professor, E-mail: hxia88@163.com

http://www.techno-press.org/?journal=sem&subpage=8 ISSN: 1225-4568 (Print), 1598-6217 (Online)

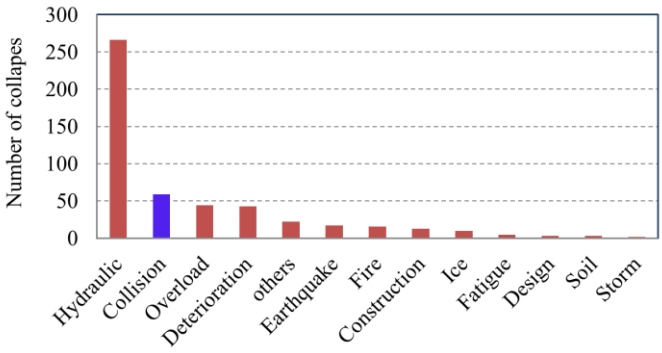

Fig. 1 Statistics of bridge collapses during 1989 to 2000

were caused by vessels, accounting for more than 60% of the total. These data fully demonstrate that the vessel collisions have become one of the main causes for bridge damage accidents.

In addition to the bridge collapse accidents, even more is the number of bridges collided by vessels but not all of them collapsed. In the United States, a total of 2418 bridges suffered vessel collisions from 1981 to 1990 (Larry and Olson 2005), while from 1992 to 2001, this number was reported as 2692 (Wuttrich *et al*. 2001).

In China, only for railway bridges, the recorded vessel collision accidents exceeded 400 times. Up to 2007, the Wuhan Yangtze River Bridge and the Nanjing Yangtze River Bridge had been collided by vessels 71 times and 28 times, respectively, in which a serious collision once interrupted the Beijing-Guangzhou railway for dozens of hours.

These bridge accidents of vessel collisions have caused serious economic loss and social influence, absorbing attentions of related researchers and designers.

When a collision load acts on a bridge pier, it may cause dislocation of bearings and girders, uneven deformation or fracture of expansion joints, and even collapse of girders, resulting in serious accidents, as studied by many researchers (Larry and Olson 2005, Wuttrich *et al*. 2001, Davidson *et al*. 2013). For high-speed railway bridges, however, even if there is no girder collapse, the vibrations and displacements induced by collision may deform the track and make it unstable, which may further threaten the running safety of the train on the bridge. When the collision is intense and the train speed is high, the running safety of the train may be seriously affected, and in the most serious case, the train may even derail from the track. As an important part of risk assessment on bridge operation safety, therefore, it is necessary to study the running safety of trains on bridges subjected to vessel collisions.

The mechanism of vessel collision with the pier or the superstructure of a bridge has been studied by many researchers, such as Consolazio *et al*. (2006), Pedersen (2010), Fan and Yuan (2012), Sha and Hao (2013), Chegenizadeh *et al*. (2014), through theoritical analysis, numerical simulation and experimental investigation.

There are many researches on the dynamic behaviors of coupled train-bridge systems, and those subjected to earthquake or wind actions, such as Yau and Frýba (2007), Liu *et al*. (2009), Deng and Cai (2010), Au *et al*. (2011), Xia *et al*. (2011), Zhai *et al*. (2013), Rezvani *et al*. (2013). However, up to the present, only a few published papers (Laigaard Jensen *et al*. 1996, Xuan and Zhang 2001, Xia *et al*. 2011a, 2013, 2014) concerned the vibration of the train-bridge system induced by a collision and its influence on the running safety of trains, while on this problem it

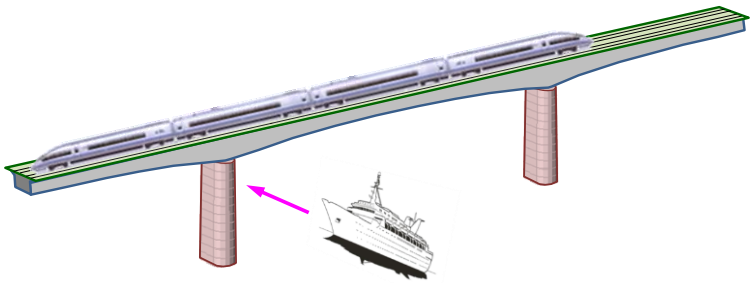

Fig. 2 A coupled train-bridge system subjected to a vessel collision

lacks of specialized research on a vessel caused collision. To this end, this paper presents an analysis model, and analyzes the dynamic responses of coupled train-bridge system subjected to a vessel collision. A continuous steel truss arch bridge is considered as an illustrating case study. With the vessel collision acting on the pier, the displacements and accelerations at the pier-top and the mid-span of the bridge are calculated when a CRH2 high-speed train running through the bridge, and the influence of bridge vibration on the running safety indices of the train, including derailment factors, offload factors and lateral wheel/rail forces, are analyzed.

2. Train-bridge model subjected to a vessel collision load

2.1 Dynamic analysis model of train-bridge system with collision load

When a bridge is collided by a vessel, a car or other colliding object, the analysis model of the train-bridge system can be regarded as a spatial dynamic system composed of three subsystems, the bridge subsystem, the train subsystem and the colliding object subsystem, as shown in Fig. 2.

Theoretically, the equations-of-motion for such a system can be expressed as

$$\begin{bmatrix} \mathbf{M}_{vv} & 0 & 0 \\ 0 & \mathbf{M}_{bb} & 0 \\ 0 & 0 & \mathbf{M}_{cc} \end{bmatrix} \begin{Bmatrix} \ddot{\mathbf{X}}_v \\ \ddot{\mathbf{X}}_b \\ \ddot{\mathbf{X}}_c \end{Bmatrix} + \begin{bmatrix} \mathbf{C}_{vv} & \mathbf{C}_{vb} & 0 \\ \mathbf{C}_{bv} & \mathbf{C}_{bb} & \mathbf{C}_{bc} \\ 0 & \mathbf{C}_{cb} & \mathbf{C}_{cc} \end{bmatrix} \begin{Bmatrix} \dot{\mathbf{X}}_v \\ \dot{\mathbf{X}}_b \\ \dot{\mathbf{X}}_c \end{Bmatrix} + \begin{bmatrix} \mathbf{K}_{vv} & \mathbf{K}_{vb} & 0 \\ \mathbf{K}_{bv} & \mathbf{K}_{bb} & \mathbf{K}_{bc} \\ 0 & \mathbf{K}_{cb} & \mathbf{K}_{cc} \end{bmatrix} \begin{Bmatrix} \mathbf{X}_v \\ \mathbf{X}_b \\ \mathbf{X}_c \end{Bmatrix} = \begin{Bmatrix} \mathbf{F}_{vb} \\ \mathbf{F}_{bv} + \mathbf{F}_{bc} \\ \mathbf{F}_{cb} \end{Bmatrix} \tag{1}$$

where, $\mathbf{M}$, $\mathbf{C}$ and $\mathbf{K}$ are the mass, damping and stiffness matrices of the train-bridge system, $\mathbf{X}$, $\dot{\mathbf{X}}$ and $\ddot{\mathbf{X}}$ are the displacement, velocity and acceleration vectors, with the subscripts *v*, *b* and *c* representing the train, bridge and colliding object, respectively. $\mathbf{F}_{vb}$ and $\mathbf{F}_{bv}$ are the inter-force vectors of the bridge to the train and the train to the bridge, and $\mathbf{F}_{bc}$ and $\mathbf{F}_{cb}$ are the inter-force vectors of the colliding object to the bridge and the bridge to the colliding object, respectively.

It should be noticed that the colliding object may produce plastic deformation during the collision, and the bridge may be damaged if the collision load is sufficiently large. In this case, the structural characteristics of the colliding object and the bridge may be changed, so the influence of nonlinear factors on the stiffness matrices $\mathbf{K}_{bb}$, $\mathbf{K}_{bc}$, $\mathbf{K}_{cb}$ and $\mathbf{K}_{cc}$ related to the colliding object and the bridge in Eq. (1) should be considered.

However, the coupling vibration of train-bridge system under collision load is a complex problem. The complexity contains: the characteristics of the collision load, whatever it is induced

by vessel, vehicle, ice sheet or other colliding objects, not only relate with the mass and motion speed of the colliding object, but also depend on the stiffness of the colliding object and the collided structure; and the stiffness of the colliding object is related with its own material and structural characteristics, such as the material and the structure of the vessel bow and the anti-collision beam of the vehicle, and the hardness and shape of the ice sheet. The colliding object and the collided object with different stiffness have different deformation and energy absorption capacities, which directly influence the time history characteristic of the collision load, such as the duration time and collision strength. Therefore, synchronously considering the interactions between train and bridge and between colliding object and collided structure makes the problem extremely complicated, which is almost unrealizable with the current analysis method.

On the other hand, according to the existing researches, there are three methods to obtain the collision load: field test, model experiment and numerical simulation. Whatever which method is used, the time history of the acquired collision load has included the influence of the stiffness and the deformation of the colliding object and the collided structure, and also the dynamic interaction between them. With a known collision load, it is feasible to use a simplified method to analyze the dynamic responses of train-bridge system under collision load: by neglecting the interaction between the colliding object and the bridge structure, the time history of the collision load is directly taken as the input excitation on the train-bridge system, to solve the problem through simulation analysis.

The train-bridge interaction dynamic analysis model established by this method is shown in Fig. 3, which consists of two subsystems, the train subsystem and the bridge subsystem, and the collision load is directly applied on the bridge structure as the external force $F_c(t)$.

In the analysis, the train subsystem model is established by the rigid-bodies with elastic connections, and the bridge subsystem model is established either by the FEM (Finite element method) or the MDM (modal decomposition method). The two subsystems are coupled by the

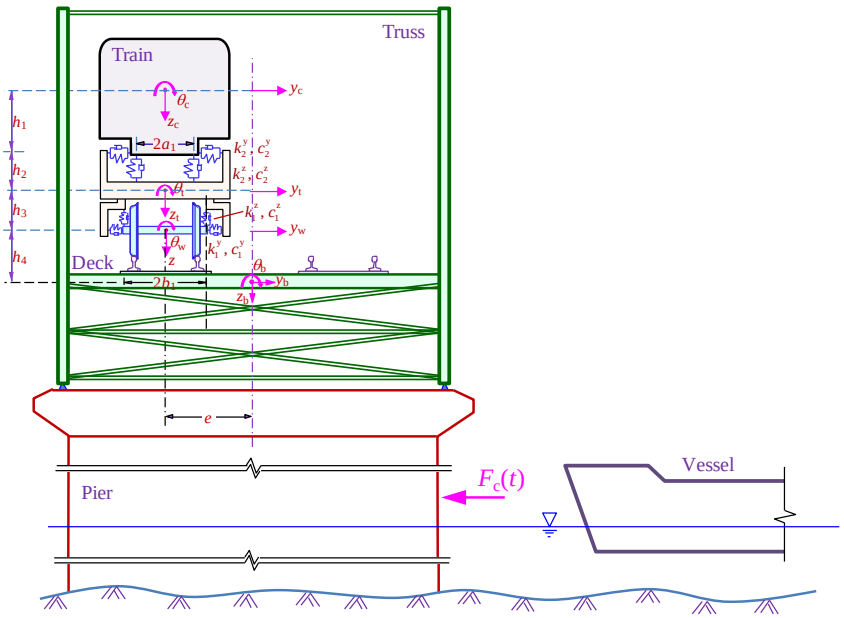

Fig. 3 Dynamic model for train-bridge system subjected to a vessel collision

wheel-rail interaction, and the track irregularity is regarded as the internal excitation of the two subsystems. When the bridge subsystem is established by the FEM, the coupled equations-of-motion for the train-bridge dynamic system subjected to collision load can be expressed as

$$\begin{bmatrix} \mathbf{M}_{vv} & 0 \\ 0 & \mathbf{M}_{bb} \end{bmatrix} \begin{Bmatrix} \ddot{\mathbf{X}}_v \\ \ddot{\mathbf{X}}_b \end{Bmatrix} + \begin{bmatrix} \mathbf{C}_{vv} & \mathbf{C}_{vb} \\ \mathbf{C}_{bv} & \mathbf{C}_{bb} \end{bmatrix} \begin{Bmatrix} \dot{\mathbf{X}}_v \\ \dot{\mathbf{X}}_b \end{Bmatrix} + \begin{bmatrix} \mathbf{K}_{vv} & \mathbf{K}_{vb} \\ \mathbf{K}_{bv} & \mathbf{K}_{bb} \end{bmatrix} \begin{Bmatrix} \mathbf{X}_v \\ \mathbf{X}_b \end{Bmatrix} = \begin{Bmatrix} \mathbf{F}_{vb} \\ \mathbf{F}_{bv} \end{Bmatrix} + \begin{Bmatrix} 0 \\ \mathbf{F}_c \end{Bmatrix} \tag{2}$$

where: $\mathbf{M}$, $\mathbf{C}$, and $\mathbf{K}$ are the mass, damping and stiffness matrices, $\mathbf{X}$, $\dot{\mathbf{X}}$ and $\ddot{\mathbf{X}}$ are the displacement, velocity and acceleration vectors, with the subscripts "*v*" and "*b*" representing the train and the bridge, respectively; F_{vb} and F_{bv} are the inter-force vectors of the bridge structure and the train vehicles, respectively. Details of these matrices and vectors can be found in the authors' previous work (Zhang *et al*. 2010, Xia *et al*. 2011b).

Since quite a lot of calculation freedoms in the FE model of the bridge may lead to a heavy calculation work, the modal decomposition technique is used for the bridge model. Firstly, the free vibration frequencies and modes of the bridge are calculated. Upon the orthogonality of the modes, the coupled FEM equations can be uncoupled, which makes the bridge response become the superposition of independent modal contributions. Owing to the fact that the dynamic response is dominantly influenced by its several lowest modes, this approach has a great advantage that an adequate estimation of the dynamic response can be obtained by considering only a certain number of vibration modes, reducing significantly the computational effort. When the bridge subsystem model is established by the MDM, the motion equation of the system can be express as

$$\begin{bmatrix} \mathbf{M}_{vv} & 0 \\ 0 & \mathbf{M}_{bb} \end{bmatrix} \begin{Bmatrix} \ddot{\mathbf{X}}_v \\ \ddot{\mathbf{Q}}_b \end{Bmatrix} + \begin{bmatrix} \mathbf{C}_{vv} & \mathbf{C}_{vb} \\ \mathbf{C}_{bv} & \mathbf{C}_{bb} \end{bmatrix} \begin{Bmatrix} \dot{\mathbf{X}}_v \\ \dot{\mathbf{Q}}_b \end{Bmatrix} + \begin{bmatrix} \mathbf{K}_{vv} & \mathbf{K}_{vb} \\ \mathbf{K}_{bv} & \mathbf{K}_{bb} \end{bmatrix} \begin{Bmatrix} \mathbf{X}_v \\ \mathbf{Q}_b \end{Bmatrix} = \begin{Bmatrix} \tilde{\mathbf{F}}_{vb} \\ \tilde{\mathbf{F}}_{bv} \end{Bmatrix} + \begin{Bmatrix} 0 \\ \tilde{\mathbf{F}}_c \end{Bmatrix} \tag{3}$$

where: $\mathbf{Q}_b$, $\dot{\mathbf{Q}}_b$ and $\ddot{\mathbf{Q}}_b$ are the modal displacement, velocity and acceleration vectors of the bridge subsystem, respectively; $\tilde{\mathbf{F}}_{vb}$ and $\tilde{\mathbf{F}}_{bv}$ are the inter-force vectors of the train vehicle and the bridge subsystem with modal coordinates. The modal displacement $\mathbf{Q}_b$ can be acquired using the following transform formula

$$\mathbf{Q}_b = \begin{bmatrix} q_1 & q_2 & \cdots & q_n & \cdots & q_{N_b} \end{bmatrix} = \mathbf{\Phi}^T \mathbf{X}_b \tag{4}$$

$$q_n = \sum_{k=1}^{N} \phi_n(k) X(k) \tag{5}$$

where: q_n is the nth modal coordinate of the bridge, $\mathbf{\Phi}$ is the mode-shape matrix of the bridge, $\phi_n(k)$ is the value of the *n*th modal function of the bridge at the *k*th node, N_b is the number of the bridge modes concerned; $X(k)$ is the displacement of the bridge at the *k*th node, and N is the total number of bridge nodes.

According to the related design codes in China, for the bridge pier and abutment located in a navigable river or a river with floating object, the collision by the vessel or the floating object should be considered in the design. For the bridge across a railway or highway, the collision on the pier and abutment by the vehicle should also be considered. In a general design, the collision load can be calculated by the related equations in the codes. In the present bridge code, however, the calculation method for the collision load is still at the static design stage, which cannot be used directly in calculating the dynamic response of the train-bridge system subjected to a collision load. Instead, the time history of thecollision load is needed, which is input to the train-bridge

system as an external excitationto take the simulation calculation.

When the bridge model is established by the FEM, the collision load on the bridge can be applied to the related structural nodes as a collision load vector $\mathbf{F}_c$. When the bridge model is established by the MDM, the generalized collision load vector $\tilde{\mathbf{F}}_c$ corresponding to the related modes can be expressed as

$$\tilde{\mathbf{F}}_c = \mathbf{\Phi}^T \mathbf{F}_c = [f_{c1}(t), f_{c2}(t), \cdots f_{cn}(t), \cdots f_{cN_b}(t)]^T \tag{6}$$

where: f_{cn} is the generalized collision force acting on the bridge corresponding to the nth mode. Suppose the collision forces act horizontally on the pier, f_{cn} can be expressed as

$$f_{cn} = \sum_{k=1}^{N} \phi_n^h(k) F_k(t) \tag{7}$$

where: $\phi_n^h(k)$ is the function value of the nth mode shape in horizontal direction of the bridge at the kth node; $F_k(t)$ is the collision force history of the vessel on the bridge at the kth node, which is only different from zero at the pier nodes affected by the collision.

2.2 Vessel collision load

For the vessel collision load, some simplified static empirical formulae are usually used in bridge design, such as in AASHTO (2007) of the United States, Eurocode 1 (2007) of Europe, FCDRB (2005) of China, and so on. Referring to these formulae, the collision force on bridge pier is related to the collision angle, collision speed, vessel type, size and tonnage. In the Eurocode 1, a half-sine-wave pulse for F_{dyn}<5 MN (elastic impact) and a trapezoidal pulse for F_{dyn}>5 MN (plastic impact) are provided for dynamic analysis. These design loads, however, do reflect the real variation properties of the impact force with the time, thus they cannot be directly used in the vibration analysis of train-bridge system subjected to vessel collision load.

Vessel collision to bridge pier is a complex nonlinear dynamic process with a huge energy exchange within a short time, which produces dynamic impulse loads varying with time. These dynamic loads can be obtained via numerical simulation or experiment. Comparatively, experiment is a reliable way to acquire the collision loads between a vessel and a pier, but due to the high cost, long operation time, and other causes, the full-size vessel-bridge collision test is extremely difficult.

According to the wave propagation theory, the impact load is generated on the interface between the vessel and the bridge, forming a complex dynamic interaction process, which is related with the material and structural characteristics of the vessel and the bridge, and the involved boundary conditions. In this sense, the nonlinear dynamic numerical simulation is a good solution for this problem. With the progress of computer hardware and structural analysis software, this simulation method has been favored by more and more researchers, such as Hu *et al*. (2005), Yan (2006), Wang and Chen (2007), Wang *et al*. (2008), Thilakarathna *et al*. (2010), Fan and Yuan (2012), and has achieved many results.

Yan (2006) carried out a systematical analysis on the vessel-bridge collision forces, concerning the mass and tonnage of vessel, impact velocity, impact angle, the shape and size of piers and platforms, and so on. He adopted the LS-DYNA software to simulate the vessel-bridge collision, and obtained some time histories of collision force. Shown in Fig. 4(a) and (b) are, respectively, the simulated collision force time histories of a 5000 DWT bulk carrier with the pier of a

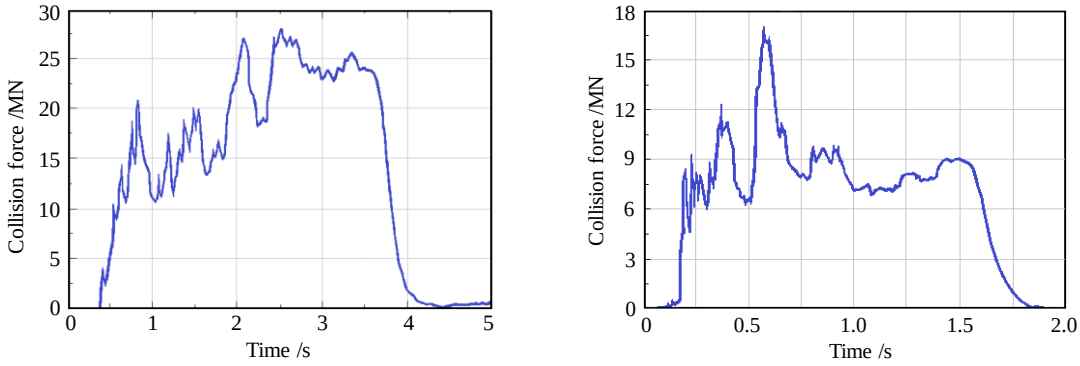

(a) 5000 DWT vessel, V_c=4.0 m/s (b) 3000 DWT vessel, V_c=3.0 m/s

Fig. 4 Collision force time histories of vessels with concrete piers

(95+3×180+95) m continuous rigid-frame bridge at the speed of 4.0 m/s and a 3000 DWT one at the speed of 3.0 m/s.

The curves in Fig. 4 indicate that the collision loads of vessel with pier are very complex. In general, the time histories of the two vessel collision loads in Fig. 4 show a characteristic of strong nonlinear wave, the duration time of which lasts about 2s~3s.

In this study, the time history of the vessel collision load shown in Fig. 4(b) is used as the external load input to the train-bridge system model.

2.3 Solution method of the system

When the collision load is known as an external load (for instance, a rough estimate of two potential collision loads in Fig. 4), the equations-of-motion for the train-bridge interaction system subjected to this collision load can be solved by the software for dynamic analysis of train-bridge interaction system.

When the train runs on the bridge, the acting positions of the inter-forces between the bridge and the train vehicles are always varying, which makes Eq. (2) or Eq. (3) become a second-order linear non-homogeneous differential equations with time-varying coefficients. In this study, these equations are solved using the Newmark implicit step-by-step integration algorithm with β=1/4. Details of the solution can be found in the authors' previous work (Zhang *et al*. 2010, Xia *et al*. 2011b).

3. Case study

A long-span rail-cum-road bridge is considered as an illustrating case study, and a vessel collision load is taken as the collision load, to analyze the dynamic response of the train-bridge system.

3.1 Bridge parameters

The main bridge consists of (180+216+180) m continuous truss girders stiffened with flexible

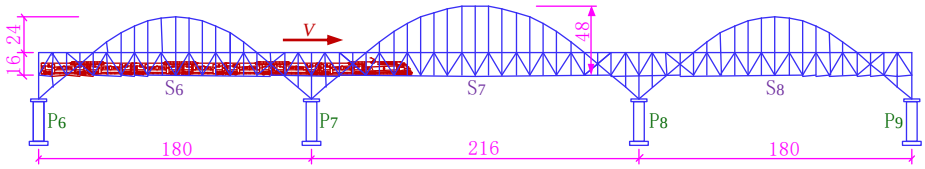

(a) Span arrangement of the main spans (Unit: m)

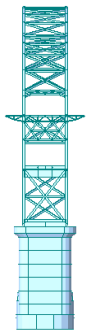

(b) Side view

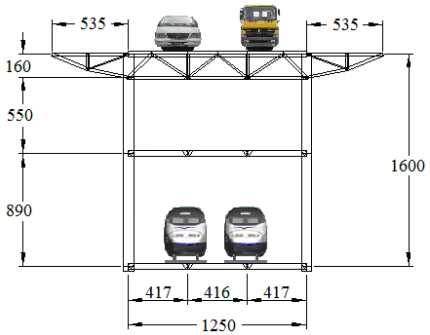

(c) Railway and road way decks (Unit: cm)

Fig. 5 Configuration of the (180+216+180) m continuous trussed arch bridge

Table 1 Stiffnesses of bridge pier foundations of the main bridge

R_x /(kN/m)	R_y /(kN/m)	R_z /(kN/m)	M_x /(kN.m/rad)	M_y /(kN.m/rad)	M_z /(kN.m/rad)
1.12E+10	1.12E+10	4.07E+10	1.384E+12	8.959E+11	5.967E+11

arches, which is connected with (2×126 m) continuous steel truss girders on the one side and multi-span 40 m simply-supported PC girders on the other side. The elevation and side view of the main bridge configurations are shown in Fig. 5.

The continuous steel truss girder consists of triangle truss with diagonal and vertical members. The height of the main truss is 16 m, and the panel interval is 9 m. The height of the stiffening arches are 32 m at the middle span, and 24 m at two side-spans. The center-to-center distance between the two main trusses is 12.5 m.

The longitudinal bracing systems are installed between the arch ribs and the chord members of the two main trusses. The transverse bracing systems are installed at every other panel nodes. In the area of the stiffening chord, the lateral coupling system is installed at each node interval, and also at the portal frames.

Located on the lower chord deck of the truss girder is the double-track railway, where the stringer-and-crossbeam system and open floor are adopted, and on the upper chord of the truss girder is the four-lane roadway, where the precast lightweight ceramsite RC slabs are installed on the steel stringers stacked on the transverse beams.

The bridge piers adopt round-end section, with the dimensional size of 5.6 m×15.6 m. The heights from pier top to the platform bottom of the piers P_6~P_9 are 30.6 m, 27.1 m, 25.6 m and 24.1 m, respectively. The stiffnesses of the piers at bottom are shown in Table 1, in which R_x, R_y, R_z are translational stiffnesses in longitudinal, transverse and vertical directions, and M_x, M_y and M_y are rotational stiffnesses about the longitudinal, transverse and vertical axes of the bridge,

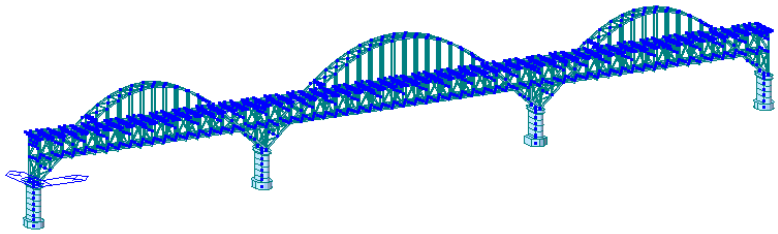

Fig. 6 FE model of the continuous trussed arch bridge

Table 2 Natural vibration properties of the bridge

Mode order	Calculated freq. /Hz	Mode-shape characteristics
1	0.471	Lateral symmetric bending of the main middle span
2	0.551	longitudinal-and-vertical bending of arch and truss
3	0.561	Lateral anti-symmetric bending of the three main spans
4	0.575	Lateral symmetric bending of the three main spans
5	1.089	Vertical bending of the right side span
6	1.108	Torsion of the middle main span with arch and truss in phase
7	1.133	Second order anti-symmetric lateral bending of the main spans
8	1.309	Vertical bending of the left side span
9	1.328	Lateral symmetric torsion of the two side spans in phase
10	1.355	Lateral anti-symmetric torsion of the two side spans out of phase

respectively.

The steel pivot type bearings are installed at fulcrums of the trussed arch, in which the fixed bearing is installed on the pier *P*7 to bear the longitudinal reaction force.

The secondary dead load on the open railway deck contains the weights of the double-tracks, the sidewalks, the refuge platform and the railing, which is 26.22 kN/m in total calculated by the designer. The width of the roadway deck is 14m, and the secondary dead load on the roadway deck includes the lightweight RC slab with the thickness of 15 cm (35.7 kN/m), the asphalt concrete pavement with the thickness of 7 cm (23.52 kN/m), the lightweight RC sidewalk slab with the thickness of 10 cm (6.8 kN/m), and the total dead load is calculated as 66.02 kN/m.

3.2 Free vibration property analysis of the bridge structure

The FE model of the bridge is established by using the software of MIDAS, as shown in Fig. 6. In modeling the bridge, all members are assumed to conform small deformation hypothesis within linear range, in which rod elements are adopted for the truss members, while bending beam elements for the transverse beams, stringers, piers, upper and lower bracing system members, using the dimensions and material parameters for the members and the pier foundation stiffness parameters provided by the designer, and the constraint conditions between the bridge piers and girders are achieved by the master-and-slave nodes. There are totally 1923 nodes, and 4651 elements for the FE model of the main bridge spans.

By a finite element modal analysis, the natural vibration characteristics including frequencies

and mode-shapes of the bridge are obtained. There are several methods including some updated ones (Cowan *et al*. 2015, Fan *et al*. 2015) available to determine the number of the modes needed when the modal decomposition technique is used. In this case study, the number of bridge modes considered in the calculation was determined according to the principle by gradually increasing the mode number until the inclusion of several additional modes no longer significantly increased the magnitudes of the responses. Following this principle, the first 30 modes are used in the calculation. The natural frequencies and the mode-shape descriptions of the first ten vibration modes are listed in Table 2.

It can be seen from Table 1 that the natural frequencies of the first 10 modes of the bridge are between 0.471~1.354 Hz, and the intervals between the modes are very small. The first mode is lateral symmetric bending of the main middle span with the frequency 0.471 Hz. The second mode is longitudinal-and-vertical bending of arch and truss with the frequency 0.551 Hz; the first tortional mode is the 9th mode of the bridge with the frequency 1.328 Hz.

In the analysis, the damping ratios are taken as 0.005 for the modes corresponding to the steel superstructure, and 0.02 for the modes corresponding to the concrete piers and foundations, respectively.

3.3 Train parameters

The high-speed train CRH2, which was used for the dynamic analysis of high-speed railway bridges and now is in service on the high-speed railway lines in China, is adopted for calculation. The CRH2 is an EMU train composed of (3M+1T)×3 cars, with M representing the motor-car and T the trailer-car, respectively. The average axle loads are 132.44 kN for the motor car and 117.72 kN for the trailer-car. Fig. 7 illustrates the first three cars of the train with the main axle interval parameters.

The track vertical, lateral and rotational irregularities are taken into consideration by using the data measured on the Qinhuangdao-Shenyang High-speed Railway in China (Zhang *et al*. 2010).

3.4 Dynamic analysis of the train-bridge system subjected to vessel collision

By using the established analysis model, the whole histories of the train passing through the (180+216+180) m continuous steel trussed-arch bridge are simulated, in which two cases with and without vessel collision on the bridge pier are considered. The integration time step is taken as 0.0002s.

In the case with collision, the force time history in Fig. 4(b) is used as the collision load, with the maximum collision force normalized as 10MN, i.e., the maximum force is adjusted to 10 MN, while keeping the shape and the duration time of the curve unchanged. In the dynamic analysis, the time history of the load is applied on pier *P*7 at 10.0 m above the platform of its foundation, when the train arrives at middle of the first main span (S_6).

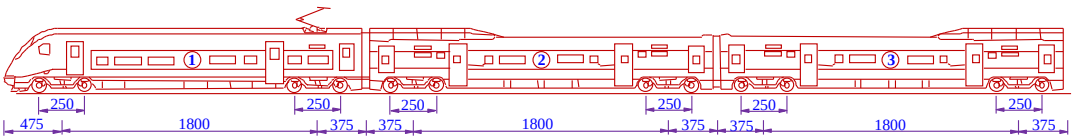

Fig. 7 Composition and main dimensions of the CRH2 train (unit: cm)

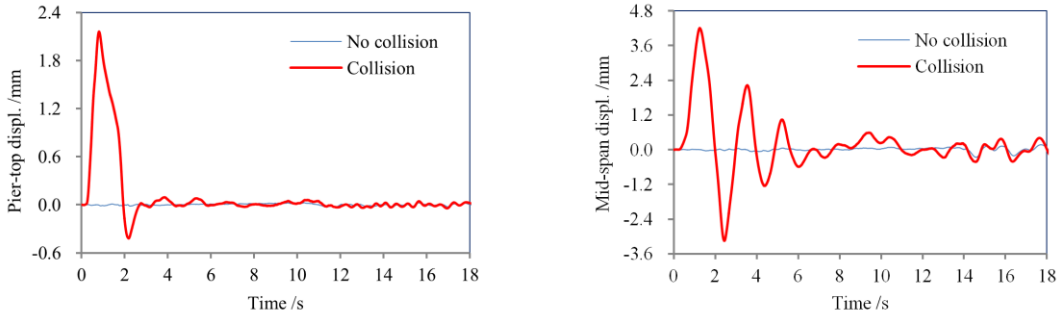

(a) At the P_7 pier-top (b) At the 216 m mid-span

Fig. 8 Lateral displacement histories of the bridge (V=200 km/h)

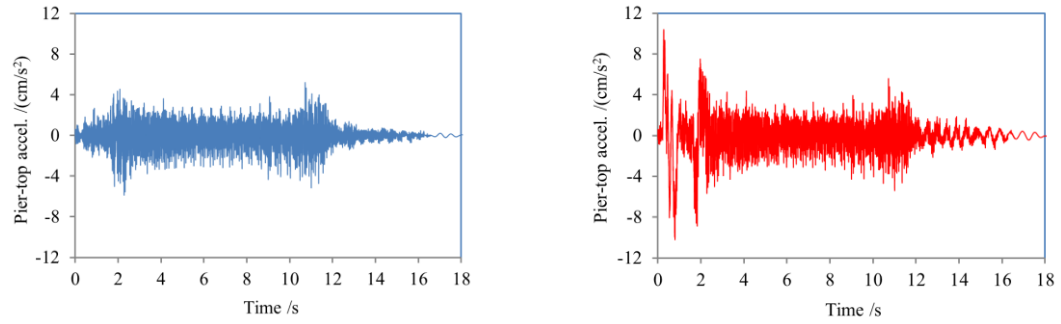

(a) No collision (b) With collision

Fig. 9 Lateral acceleration histories of the bridge at the P_7 pier-top (V=200 km/h)

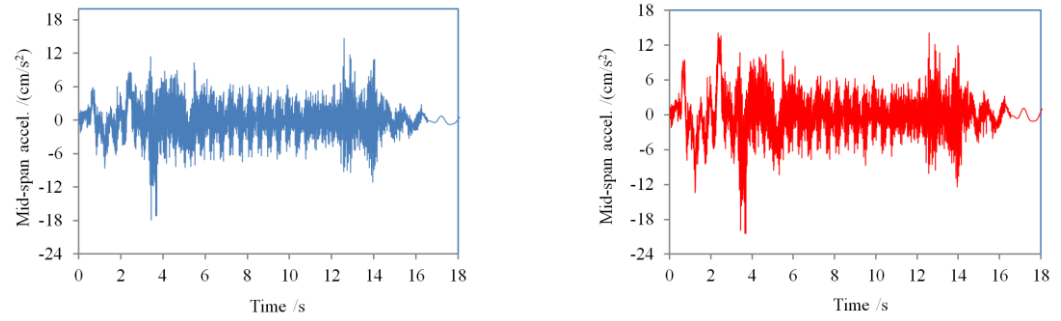

(a) No collision (b) With collision

Fig. 10 Lateral acceleration histories of the bridge at the 216 m mid-span (V=200 km/h)

3.4.1 Dynamic responses of the bridge

Illustrated in Figs. 8 to 10 are, respectively, the lateral displacement and acceleration time histories at the top of pier P_7 and the mid-span of the 216 m span (S_7) of the bridge without and with collision load, when the CRH2 train travels on the bridge at V=200 km/h.

It can be seen from the figures that the vessel collision has an obvious effect on the lateral responses of the bridge, which can be summarized as follows:

In the case without collision, the lateral responses of the bridge are induced by the running train only, therefore the time history curves are steady, with small amplitudes in both the displacements and the accelerations. For the pier-top and the mid-span, the peak displacements are 0.03 mm and 0.26 mm, and the peak accelerations are 5.87 cm/s^2 and 17.91 cm/s^2, respectively.

In the case with the vessel collision load, the lateral responses of the bridge are greatly amplified. For the displacements, the peak values are 2.16 mm at the pier-top and 4.21 mm at the mid-span, which are respectively 72 and 16.2 times of those in the case without collision. At the pier-top, the strong shock vibration lasts about 2s, almost the same duration as the collision load. While at the mid-span, the shock vibration continued a longer time, and disappears at about 7s, due to the small damping of the steel girder.

Since the collision load directly acts on the pier, the acceleration at the pier-top is much more greatly affected than that at the mid-span. The maximum accelerations are enlarged by the collision to 10.42 cm/s^2 at the pier-top and 20.45 cm/s^2 at the mid-span, respectively 1.78 and 1.14 times of those in the case without collision. Owing to the damping action of the bridge, the shock acceleration waves induced by the collision last for a very short time, and after the collision finished, the acceleration curves return very soon to their steady state similar to the case without collision.

3.4.2 Dynamic responses of the train vehicles

According to the Chinese design code, the evaluation indices for the running safety of high-speed trains include derailment factor, offload factor and lateral wheel-rail force. The expressions and the related allowable values of these indices are follows

$$\begin{aligned} &\text{Derailment factor:} && Q/P_1 = F_{\mathrm{h}ijl}/F_{\mathrm{v}ijl} \le 0.8 \\ &\text{Offload factor:} && \Delta P/\bar{P} = (P_{\mathrm{st}} - F_{\mathrm{v}ijl})/P_{\mathrm{st}} \le 0.6 \\ &\text{Wheel/rail force:} && Q = F_{\mathrm{h}ijl} \le 0.85(10 + P_{\mathrm{st}}/3) \end{aligned} \tag{8}$$

where: Q=F_{hijl} is the lateral wheel-rail force, P_1=$F_{\mathrm{v}ijl}$ is the vertical force of the wheel at the climbing-up-rail side, ΔP is the offloaded vertical wheel-rail force, $\bar{P} = P_{\mathrm{st}}$ is the average vertical static load of the two wheels on a wheel-set.

The lateral and vertical wheel-rail forces can be calculated by the following equations

$$\begin{aligned} F_{\mathrm{h}ijl} = &-m_{\mathrm{w}ijl}\ddot{Y}_{\mathrm{w}ijl} + c^{\mathrm{y}}_{1ij}(\dot{Y}_{\mathrm{t}_j i} - h_{3i}\dot{\theta}_{\mathrm{t}_j i} + 2\eta_{jl}d_i\dot{\psi}_{\mathrm{t}_j i} - \dot{Y}_{\mathrm{w}ijl}) \\ &+ k^{\mathrm{y}}_{1ij}(Y_{\mathrm{t}_j i} - h_{3i}\theta_{\mathrm{t}_j i} + 2\eta_{jl}d_i\psi_{\mathrm{t}_j i} - Y_{\mathrm{w}ijl}) \end{aligned} \tag{9}$$

$$\begin{aligned} F_{\mathrm{v}ijl} = &-m_{\mathrm{w}ijl}\ddot{Z}_{wijl} + c^{\mathrm{z}}_{1ij}(\dot{Z}_{\mathrm{t}_j i} + 2\eta_{jl}d_i\dot{\varphi}_{\mathrm{t}_j i} - \dot{Z}_{\mathrm{w}ijl}) + k^{\mathrm{z}}_{1ij}(Z_{\mathrm{t}_j i} + 2\eta_{jl}d_i\varphi_{\mathrm{t}_j i} - Z_{\mathrm{w}ijl}) \\ &+ g[m_{\mathrm{w}ijl} + (0.5M_{\mathrm{c}i} + M_{\mathrm{t}ij})/2] \end{aligned} \tag{10}$$

where, F_{hijl} and F_{vijl} are the lateral and vertical wheel/rail forces of the lth wheel at the jth bogie of the ith car-body, respectively. Y_{tji}, θ_{tji}, ψ_{tji}, Z_{tji} and φ_{tji} represent the lateral, rolling, yawing, vertical and pitching displacements of the jth bogie of the ith car-body, respectively. M_{ci} is the mass of the ith car-body, M_{tij} is the mass of the jth bogie of the ith car-body, and g is the gravity acceleration. Details of these symbols can be seen in Fig. 3 and the authors' previous works (Zhang *et al*. 2010, Xia *et al*. 2011b).

The allowable lateral wheel-rail forces for the motor-car and the trailer-car of the CRH2 high-speed train are 46.03 kN and 41.85 kN, corresponding to their static loads of 132.4 kN and 117.7

kN, respectively.

Shown in Figs. 11-13 are, respectively, the time history curves of derailment factor, offload factor and lateral wheel/rail force of a motor-car wheel-set on the CRH2 train when it travels on the bridge at *V*=200 km/h, with no collision load and the vessel collision load acting on the bridge pier.

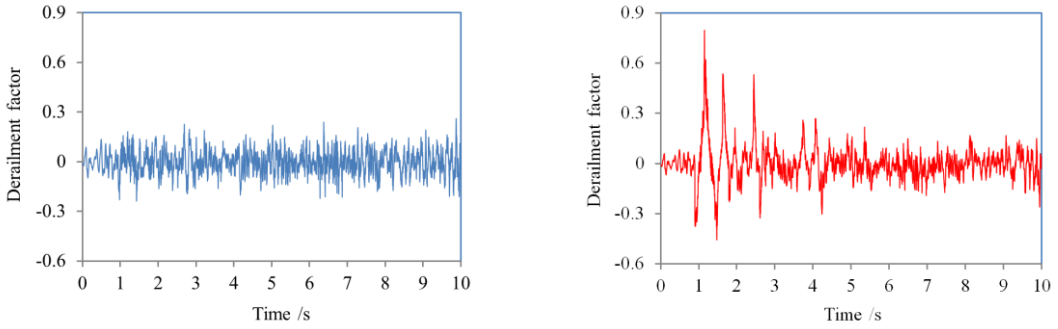

(a) No collision (b) With collision

Fig. 11 Time histories of the derailment factor (*V*=200 km/h)

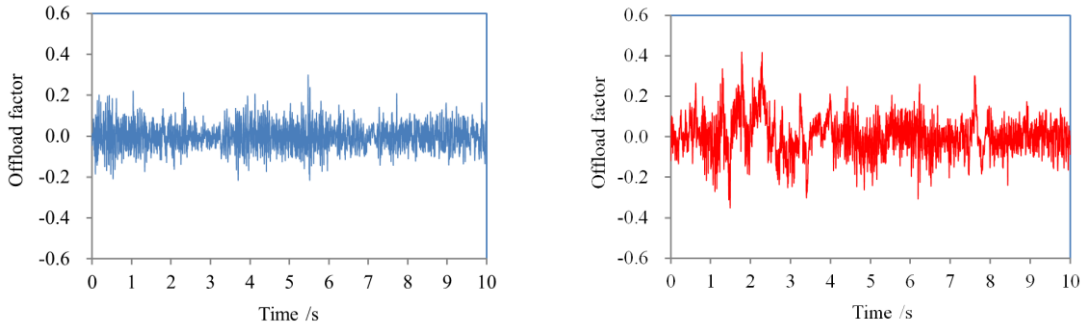

(a) No collision (b) With collision

Fig. 12 Time histories of the offload factor (*V*=200 km/h)

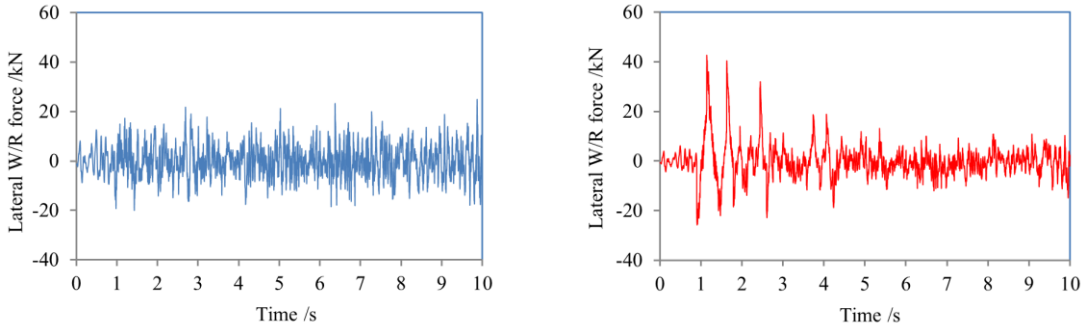

(a) No collision (b) With collision

Fig. 13 Time histories of the lateral wheel/rail force (*V*=200 km/h)

The figures show that the running safety indices of the train are strongly affected by the collision action. Without the collision, variations of these running safety indices are affected by the running train only, therefore the time history curves are rather steady, and the peak derailment factor is 0.262, the peak offload factor is 0.299 and the peak lateral wheel/rail force is 20.09 kN.

When the vessel collision load is applied on the bridge, there appear strong shock waveforms in the time history curves, thus the running safety indices are greatly amplified. Compared to those without collision, the peak derailment factor is enlarged to 0.797 by 203.8%, the offload factor to 0.419 by 40.1%, and the lateral wheel/rail force to 42.6 kN by 69.8%. It can be noticed that the maximum derailment factor and the lateral wheel/rail force have been very close to the corresponding allowances.

3.5 Influence of vessel collision induced bridge vibration on running safety of train

The running safety of high-speed trains on the railway bridge subjected to a vessel collision is an issue of concern in railway engineering. According to Wand and Chen (2007), Yan (2006) and Hu *et al*. (2005), the dynamic loads of vessel collision with bridge piers can be as high as dozens or even hundreds of Mega-Newton. In this section, with the same bridge, train and track irregularity parameters given in Section 3.1, the effect of a vessel collision with the bridge pier on the running safety of train is investigated by considering different collision force intensities (represented by the maximum collision force herein) and train speeds.

3.5.1 Influences of train speed and collision intensity

In the analysis, keeping the parameters of the bridge and the CRH2 train unchanged, the train speed is varied from 150 km/h to 260 km/h, and at each train speed, seventeen loading cases are considered: no collision, vessel collision loads in Fig. 4(b) with their intensities normalized as 1 MN, 2 MN, ..., 16 MN, respectively. The maximum values of running safety indices, which are taken from the corresponding time histories of all wheel-sets during each passage of the train on the bridge, are used for comparison. Shown in Fig. 14 are the distributions of maximum derailment factors, offload factors and lateral wheel/rail forces versus train speed.

From the figures for the cases without collision and with collision intensities 1-16 MN, it can be seen that the increase tendency of the train running safety indices with train speed and collision

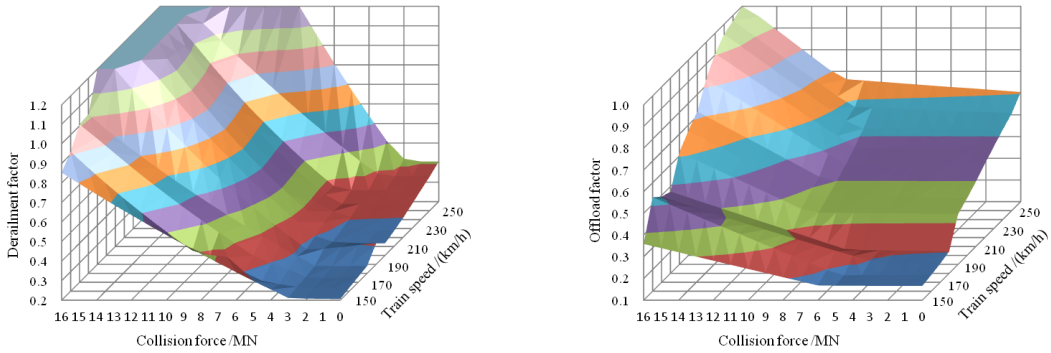

(a) Derailment factor (b) Offload factor

Fig. 14 Distributions of running safety indices vs train speed and collision intensity

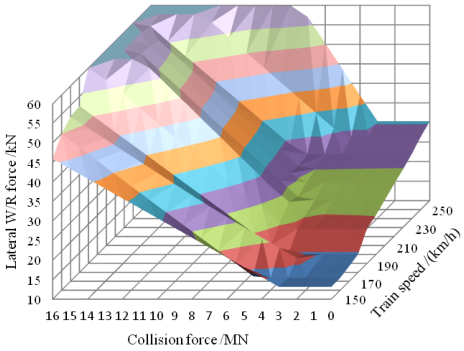

(c) Lateral *W/R* force of motor-car

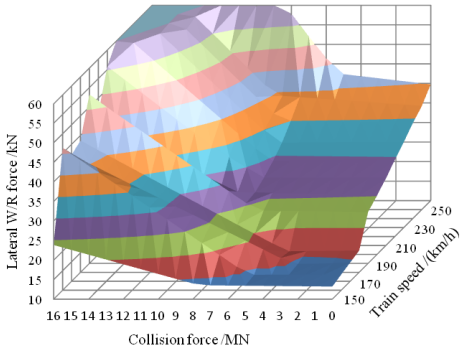

(d) Lateral *W/R* force of trailer-car

Fig. 14 Continued

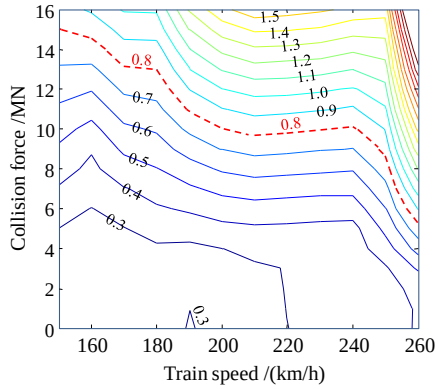

(a) Derailment factor

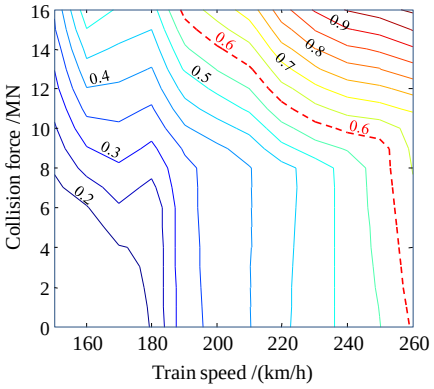

(b) Offload factor

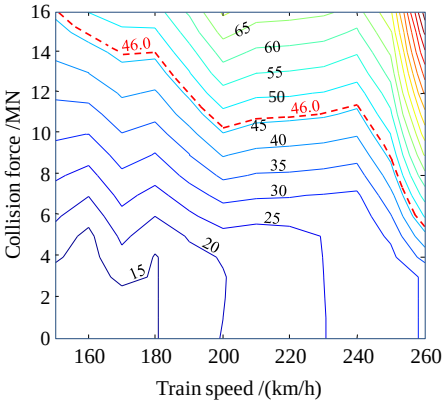

(c) Lateral *W/R* force of motor-car

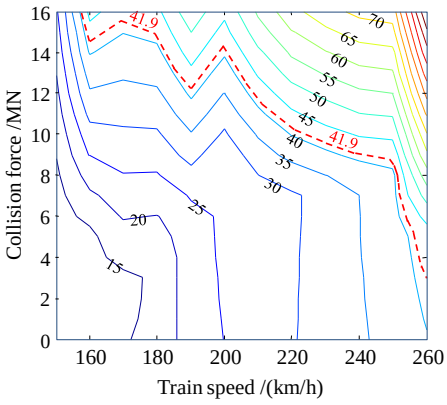

(d) Lateral *W/R* force of trailer-car

Fig. 15 Contour graphs of running safety indices vs train speed and collision intensity

intensity is obvious. Generally, the higher the train speed, and the stronger the collision intensity, the bigger the running safety indices.

For better understanding the distribution of the running safety indices versus train speed and

collision intensity, the calculated results in Fig. 14 are projected to a plane coordinate system, with the abscissa representing the train speed and the ordinate the collision intensity, to form a group of contour curves for the derailment factors, offload factors and lateral *W/R* forces versus the train speed and the collision intensity, as shown in Fig. 15.

In the figures, each curve represents a same response level for the corresponding running safety index varying with different collision intense and train speed. The thick dashed-lines in the figures define the boundaries of safety areas for the running safety of the high-speed train on the bridge subjected to collision with various intensities, which are 0.8 for the derailment factors, 0.6 for the offload factor, and approximately 46.0 kN and 41.9 kN for the lateral *W/R* forces of motor-car and trailer-car, respectively, according to the corresponding allowances given by Eq. (8).

The boundary curve in each contour graph determines the critical train speed for running safety on the bridge subjected to different collision intensities, controlled by the corresponding running safety index. According to these contour curves, for example, for a collision 10 MN, the critical train speed on the bridge is about 200 km/h when controlled by the derailment factor, while it is about 230 km/h by the offload factor, about 240 km/h by the lateral *W/R* force of motor-car, and about 220 km/h of trailer-car, respectively.

3.5.2 Evaluation of running safety of high-speed train on bridge subjected to vessel collision

The previous analyses show that collision intensity and train speed are the two main factors to control the train running safety. To ensure the running safety of trains on bridges subjected to vessel collision load, a further simulation is performed to find out a comprehensive evaluation threshold curve, which can be acquired by combining the four safety boundaries for running train in Fig. 15. By connecting the lowest critical train speeds under different collision intensities in the four indices, a comprehensive inscribed curve is formed, which is the comprehensive threshold, as shown in Fig. 16. This comprehensive curve divides the whole area into two parts. In the lower left area, all the running safety indices meet all the related allowances of Eq. (8), indicating that the running safety of the train can be ensured, while in the upper right area, at least one of the indices exceeds the related allowance, indicating that the running safety of the train cannot be guaranteed.

It can be observed from the figure that the running safety of the train are influenced by the comprehensive effect of vessel collision intensity and train speed:

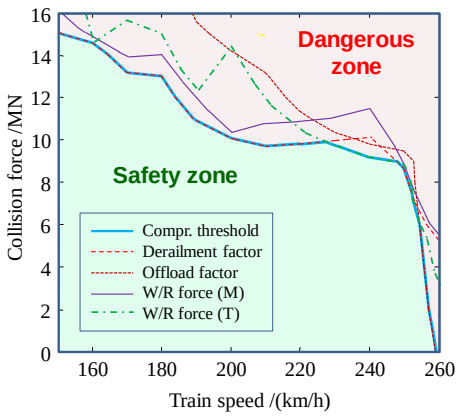

Fig. 16 Threshold curves of train speed and collision intensity

(1) The greater the collision intensity, the lower the allowable train speed for running safety. In the case without collision load, all indices meet the related allowances for the train speed up to 258 km/h. With the increase of collision intensity, the train should gradually lower its speed to ensure the running safety. For example, when the collision intensity reaches 12 MN, the train can only run safely at 180 km/h.

(2) The higher the train speed, the smaller the collision intensity that the train-bridge system can allow. At V=150 km/h, the train can run safely for a collision intensity up to 15 MN; at V=200 km/h, the allowable collision intensity is lowered to 10 MN; while when $V \geq 250$ km/h, the allowable collision intensity dropped very fast from 8 MN to zero, to ensure the running safety of the train.

4. Conclusions

A framework for performing a dynamic analysis of the train-bridge system subjected to vessel collision load was proposed. Based on the framework, an illustrative case study was carried out with a (180+216+180) m continuous trussed-arch bridge and the CRH2 EMU high-speed train, to investigate the dynamic response of the bridge subjected to a vessel collision and its influence on the running safety of high-speed train. Some conclusions can be obtained as follows.

(1) Collision load has an obvious effect on the dynamic responses of the bridge and the running train. Under the collision load, the dynamic responses of the bridge, especially the lateral displacement at the pier-top and mid-span and the lateral acceleration at the pier-top of the bridge, are much greater than those in the case without collision, exerting a great influence on the running safety of high-speed train. This effect should be fully recognized in the anti-collision design of high-speed railway bridges.

(2) Strong vessel collision may threaten the running safety of high-speed train on the bridge, which is affected by both the collision intensity and the train speed. The running safety indices, including derailment factors, offload factors and lateral wheel-rail forces, all increase with the collision intensity. Generally, the higher the train speed, the smaller the collision load that the train-bridge system can allow, while the greater the collision intensity, the lower the allowable train speed for safety. With the increase of collision force on the bridge, the train has to lower its running speed to ensure the safety.

(3) For the (180+216+180) m continuous trussed-arch bridge and the CRH2 EMU train in the case study, within the train speed range of 150~260 km/h, the maximum allowable collision intensity is 15 MN with respect to train speed 150 km/h, which decreases with the increase of train speed, and especially, the decrease rate becomes faster when the train speed is higher than 250 km/h.

Dynamic analysis of coupled train-bridge systems subjected to vessel collision load is a rather complex problem, which is related with running speed of the train, the structural form of the bridge, the intensity and acting position of the vessel collision load, and so on. In this paper, only a preliminary study is performed and illustrated by a case study. The proposed analysis framework and the calculation results may provide a reference for the dynamic design of high-speed railway bridges subjected to vessel collision.

In the framework, a collision force in the reference (Yan 2006) is adopted to the arch-trussed bridge. This is a simplified treatment for this study. In fact, vessel collision loads are dependent upon the mass and initial velocity of the impacting vessel, the stiffness of the vessel bow (or the

engaged region of the vessel), the shape and width of the impacted surface, and the stiffness/inertia of the bridge-soil system, which will be taken into account in the further study.

Moreover, the authors noticed several updated studies in analysis of barge-bridge collisions. Cowan *et al*. (2015) proposed an RSA (response-spectrum analysis) procedure for barge impact analysis of bridges, without yielding voluminous amounts of time-varying results, which is capable of directly producing maximum response parameters that are most pertinent to structural design. Fan *et al*. (2015) proposed a new modal combination rule WAS (weighted algebraic sum) for the shock spectrum analysis of barge-bridge collisions, which is more efficient and accurate in the barge-bridge collision spectrum analysis.

Herein, the authors acknowledge the works of the aforementioned references, and the method proposed by them will be incorporated in dynamic analysis of train-bridge system subjected to collision loads.

Acknowledgments

The paper is supported by the National Basic Research Program ("973" Project, Grant No. 2013CB036203), the National Natural Science Foundations (Grant No. 51308035), the Fundamental Research Funds for the Central Universities (2015RC006) of China, and the project by the CCCC Highway Consultants CO., Ltd.

References

AASHTO (2007), *Load and Resistance Factor, LRFD Bridge Design Specifications*, American Association of State Highway and Transportation Officials, Washington, D.C.

Au, F.T.K., Lou, P., Li, J., Jiang, R.J., Zhang, J., Leung, C.C.Y., Lee, P.K.K., Lee, J.H., Wong, K.Y. and Chan, H.Y. (2011), "Simulation of vibrations of Ting Kau Bridge due to vehicular loading from measurements", *Struct. Eng. Mech.*, **40**(4), 471-488.

Chegenizadeh, A., Ghadimi, B. and Nikraz, H. (2014), "Investigation of ship collision with floating pier structures", *Coupl. Syst. Mech.*, **3**(3), 319-327.

Consolazio, G.R., Cook, R.A., McVay, M.C., Cowan, D., Biggs, A. and Bui, L. (2006), *Barge Impact Testing of the St. George Island Causeway Bridge, Phase III: Physical Testing and Data Interpretation*, Final Rep. to FDOT, Contract No. BC-354, Gainsville, Fla.

Cowan, D.R., Consolazio, G.R. and Davidson, M.T. (2015), "Response-spectrum analysis for barge impacts on bridge structures", *ASCE J. Bridge Eng.*, **20**(12), 04015017.

Davidson, M.T., Consolazio, G.R., Getter, D.J. and Shah, F.D. (2013), "Probability of collapse expression for bridges subject to barge collision", *J. Bridge Eng.*, **18**(4), 287-296.

Deng, L. and Cai, C.S. (2010), "Identification of dynamic vehicular axle loads: theory and simulations", *J. Vib. Control*, **16**(14), 2167-2194.

Dong, Z.F., Guo, J. and Wang, J.J. (2009), "Review of bridge collapse and prevention measures", *Highway*, **16**(2), 30-32.

Eurocode 1 (2007), EN1991-1-7: Actions on Structures General Action, Accidental Actions.

Fan, W. and Yuan, W.C. (2012), "Shock spectrum analysis method for dynamic demand of bridge structures subjected to barge collisions", *Comput. Struct.*, **90-91**, 1-12.

Fan, W., Zhang, Y.Y. and Liu, B. (2015), "Modal combination rule for shock spectrum analysis of bridge structures subjected to barge collisions", *ASCE J. Eng. Mech.*, **142**(2), 04015083.

FCDRB (2005), *Fundamental Code for Design on Railway Bridges (TB10002.1-2005)*, The China Railway

Publishing House, Beijing. (in Chinese)
Harik, I.E., Shaaban, A.M., Gesund, H., Valli, G.Y.S. and Wang, S.T. (1990), "United States bridge failures, 1951-1988", *J. Perfor. Const. Facil.*, ASCE, **4**(4), 272-277.
Hu, Z.Q., Gu, Y.N., Gao, Z. and Li, Y.N. **(**2005), "Fast evaluation of ship-bridge collision force based on nonlinear numerical simulation", *Eng. Mech.*, **22**(3), 235-240.
Jensen, J.L., Svensson, E., Eiriksson, H.J. and Ennemark, F. (1996), "Ship-induced derailment on a railway bridge", *Struct. Eng*., **6**(2), 107-112.
Ke, Z.T. and Yang, Y.Q. (2007), "Operation properties of the Jiujiang Yangtz River Bridge", Technical Report, The China Academy of Railways. (in Chinese)
Larry, D. and Olson, P.E. (2005), "Dynamic bridge substructure evaluation and monitoring", Report No. FHWA-RD-03-089, US Federal Highway Administration.
Liu, K., De Roeck, G. and Lombaert, G. (2009), "The effect of dynamic train-bridge interaction on bridge response during a train passage", *J. Sound Vib.*, **325**, 240-251.
Pedersen, P.T. (2010), "Review and application of ship collision and grounding analysis procedures", *Marine Struct.*, **23**(3), 241-262.
Rezvani, M.A, Vesali, F. and Eghbali, A. (2013), "Dynamic response of railway bridges traversed simultaneously by opposing moving trains", *Struct. Eng. Mech.*, **36**(5), 713-734.
Sha, Y.Y. and Hao, H. (2013), "Laboratory tests and numerical simulations of barge impact on circular reinforced concrete piers", *Eng. Struct.*, **46**, 593-605.
Thilakarathna, H.M.I., Thambiratnam, D.P., Dhanasekar, M. and Perera, N. (2010), "Numerical simulation of axially loaded concrete columns under transverse impact and vulnerability assessment", *J. Impact Eng.*, **37**(11), 1100-1112.
Wang, J.J. and Chen, C. **(**2007), "Simulation of damage for bridge pier subjected to ship impact", *Eng. Mech.*, **24**(7), 156-160.
Wang, L.L., Yang, L.M., Huang, D.J., Zhang, Z.W. and Chen, G.Y. (2008), "An impact dynamics analysis on a new crashworthy device against ship-bridge collision", *J. Impact Eng.*, **35**(8), 895-904.
Wardhana, K. and Hadipriono, F.C. (2003), "Analysis of recent bridge failures in the United States", *J. Perform. Const. Facil*., ASCE, **17**(3), 144-150.
Wuttrich, R., Wekezer, J., Yazdani, N. and Wilson, C. (2001), "Performance evaluation of existing bridge fenders for ship impact", *J. Perfor. Const. Facil.*, ASCE, **15**(1), 17-23.
Xia, C.Y., Lei, J.Q., Zhang, N., Xia, H. and De Roeck, G. (2011a), "Dynamic analysis of a coupled high-speed train and bridge system subjected to collision load", *J. Sound Vib*., **331**(10), 2334-2347.
Xia, C.Y., Xia, H. and De Roeck, G. (2014), "Dynamic response of a train-bridge system under collision loads and running safety evaluation of high-speed trains", *Comput. Struct.*, **140**, 23-38.
Xia, C.Y., Xia, H., Zhang, N. and Guo, W.W. (2013), "Effect of truck collision on the dynamic response of train-bridge systems and running safety of high-speed trains", *J. Struct. Stab. Dyn.*, **13**(3), 1-18.
Xia, H, De Roeck, G. and Goicolea, J.M. (2011b), *Bridge Vibration and Controls: New Research*, Nova Science Publishers, New York.
Xuan, Y. and Zhang, D. (2001), "Derailment of train induced by vessel collision on railway bridge pier", *Int. Bridge*, **4**(2), 60-64.
Yan, H.Q. (2006), "Simulation of damage and impact forces for bridge piers subjected to ship collision", Master's Dissertation, Tongji University, Shanghai, China.
Yau, J.D. and Frýba, L. (2007), "Response of suspended beams due to moving loads and vertical seismic ground excitations", *Eng. Struct.*, **29**(12), 3255-3262.
Zhai, W.M., Xia, H. and Cai, C.B. (2013), "High-speed train-track-bridge dynamic interactions-Part I: theoretical model and numerical simulation", *Int. J. Rail Trans.*, **1**(1-2), 3-24.
Zhang, N. and Xia, H. (2010), "A vehicle-bridge linear interacted model and its validation", *J. Struct. Stab. Dyn.*, **9**(2), 335-361.